Ceramics International **24** (1998) 401–410

PII: S0272-8842(97)00028-X
0272-8842/98 $19.00+.00

Investigation on Phase Separation, Nucleation and Crystallization in Bioactive Glass-Ceramics Containing Fluorophlogopite and Fluorapatite

Xiaofeng Chen,[a]* Larry L. Hench,[a] David Greenspan,[b] Jipin Zhong[b] & Xiaokai Zhang[c]

[a]Department of Materials Science and Engineering, University of Florida, Gainesville, FL 32611, USA
[b]U.S. Biomaterials Corporation, Alachua, FL 32615, USA
[c]Analysis and Test Center, Shandong Normal University, Jinan, Shandong, 250014, People's Republic of China

(Received 19 February 1997; accepted 27 March 1997)

Abstract: Apatite and mica-containing glass-ceramics in the system K_2O–MgO–CaO–Al_2O_3–B_2O_3 SiO_2–P_2O_5–F can be used to repair and reconstruct diseased or damaged bones and teeth, due to their biocompatibility and bioactivity. Like other glass-ceramics, the properties of these machinable glass-ceramics depend on composition, size and volumetric ratios of the crystalline phases in the materials. Phase separation, nucleation and crystallisation of these multi-phase glass-ceramics were investigated with DTA, SEM/EDAX, XRD and FTIR techniques. The phase relationships are discussed with regard to crystal chemistry, thermodynamics and kinetics. © 1998 Elsevier Science Limited and Techna S.r.l. All rights reserved

1 INTRODUCTION

Bioactive glasses and glass-ceramics are very promising biomaterials which have been successfully applied to the repair and reconstruction of diseased or damaged hard tissues (bones and teeth) of humans.[1–3] Hench's studies indicate that bioactive glasses (45S5 series) and bioactive glass-ceramics belong to two different classes of bioactive implants, i.e. Class A and Class B, respectively, due to large differences in the rate of bone bonding which indicates that different biochemical factors are occurring at the implant–tissue interface. Class A bioactivity leads to osteoproduction due to both intercellular and extracellular factors. Class B bioactivity leads to osteoconduction due to extracellular factors. There is a compromise between the mechanical behaviour of bioactive implants and their level of bioactivity. Clinical applications have evolved so as to minimise this compromise.[4]

Machinable bioactive glass-ceramics containing microcrystalline phases of mica and apatite can be considered as class B bioactive implants. These glass-ceramics have good mechanical strength, fracture toughness, biocompatibility and a satisfactory degree of bioactivity although they take a longer time to bond to living bone tissue than bioactive glasses.[2,5,6] This class of glass-ceramic has a better machinability than other glass-ceramics due to the large amount of layered mica phase which is oriented randomly and distributed uniformly in the glassy matrix. Consequently, it is easier to process mica-based glass-ceramics into surgical parts with various complex shapes by using normal clinical machining methods. The surgeon can easily tailor a device to a patient during an operation.[5]

Like other glass-ceramics, the properties of machinable glass-ceramics depend on the kinds, sizes and volumetric ratios of the primary crystalline phases existing in the material. However, these textural features are critically affected by composition of the parent glasses and conditions of heat

*To whom correspondence should be addressed.

treatment. In this work, the mechanisms of phase separation, nucleation and crystallisation of the glasses in the system K_2O–MgO–CaO–Al_2O_3–B_2O_3–SiO_2–P_2O_5–F were investigated, and the interrelationship between phase separation and crystallisation was established.

2 EXPERIMENTAL

2.1 Materials preparation

The base glass compositions were selected from the system K_2O–MgO–Al_2O_3–B_2O_3–SiO_2–F. The crystalline phase of fluorophlogopite ($KMg_3(Al\text{–}Si_3O_{10})F_2$) can be formed in the base glass of this system. The chemical composition range of the base glass is shown in Table 1. Two different percentages of $CaO+P_2O_5$ ($CaO/P_2O_5=3.32$ mole ratio) were introduced into the base glass as the necessary components to form fluorapatite ($Ca_5(PO_4)_3F$) microcrystals. Samples with lower amounts of $CaO+P_2O_5$ are designated as Gl and those with higher amounts of $CaO+P_2O_5$ are designated G2; 4 wt% TiO_2 was doped into both glass batches as a nucleation agent. To investigate the effect of TiO_2 on crystallisation of the main crystalline phases, we also prepared a glass sample with the same composition as G2 but without addition of TiO_2. This glass is designated as G3. Additional amounts of CaO and P_2O_5 in glasses Gl, G2 and G3 are listed in Table 2 The above three glasses (Gl, G2 and G3) were prepared from reagent grade chemicals. The batches were put into sintered quartz crucibles and melted at 1530°C for 3 h in a $MoSi_2$ electric furnace. The resultant melts were poured onto a stainless steel plate preheated at 400°C and were then annealed at 580°C for 1 h to relax residual stresses.

Table 1. The chemical composition range of the base glass (mol%)

SiO_2	B_2O_3	Al_2O_3	MgO	MgF_2	K_2O
48–53	6–10	5–11	10–13	8–10	5–8

Table 2. CaO and P_2O_5 addition amount in Glass Gl, G2 and G3 (molar number in 100 mol base glass)

Sample I.D.	CaO	P_2O_5
G1	19.6	5.9
G2	32.6	9.8
G3*	32.6	9.8

*The composition of glass G3 was the same as glass G2, only without doping TiO_2 nucleation agent. For glasses G1 and G2, TiO_2 was doped by 4 wt% of the glass batches.

In order to crystallise the glass-ceramics, the three glasses (Gl, G2 and G3) were heat-treated in three stages determined by referencing the DTA curves of the glasses. These are illustrated, respectively, in Table 3, Figs 1 and 2.

At the end of each stage of heat treatment, one glass specimen was taken from the furnace (see Fig. 3). The specimens taken out after different periods of heat treatment were designated as follows:

Gl-0, G2-0 and G3-0: the original glasses;
Gl-1, G2-1 and G3-1: the specimens taken out after Stage l;
Gl-2, G2-2 and G3-2: the specimens taken out after Stage 2;
Gl-3, G2-3 and G3-3: the specimens taken out after Stage 3.

2.2 Microanalyses of the microstructure and primary crystalline phases

After different heat treatment stages, the specimens were observed and analysed by the following techniques:

1. SEM/EDAX (scanning electron microscope/energy-dispersive analysis of X-ray): Small pieces of the specimens with fresh sections were etched in 5% HF acid for 10 s and coated with carbon film. Micromorphologies of the specimens were observed under a

Table 3. Temperatures and times of heat treatment schedule

Glass	Stage 1	Stage 2	Stage 3
G1	650°C 1 h^{-1}	800°C 3 h^{-1}	850°C 3 h^{-1}
G2	650°C 1 h^{-1}	770°C 3 h^{-1}	930°C 3 h^{-1}
G3	650°C 1 h^{-1}	780°C 3 h^{-1}	930°C 3 h^{-1}

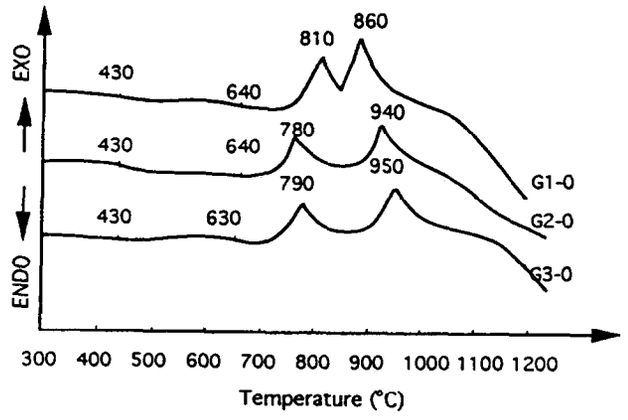

Fig. 1. The DTA curves of the glasses G1-0, G2-0 and G3-0.

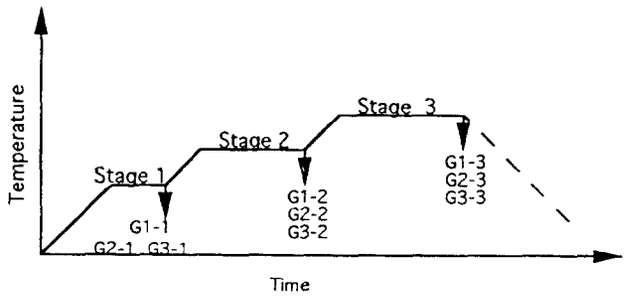

Fig. 2. The heat treatment schedules for nucleation and crys-

scanning electron microscope (Hitachi, H8010, Japan). In the meantime, the elemental distribution in different phases were analysed with EDAX device equipped in the SEM system.

2. XRD (X-ray diffraction) analysis: To identify the microcrystalline phases precipitated in the glass at different stages of heat treatment, the glass-ceramic specimens corresponding to each heat treatment stages were ground into fine powder in an agate mortar and then, analysed with powder X-ray diffraction technique (Rigaku, D-9C, CuKα, 140KV, 30mA, Japan).
3. FTIR (Fourier transform infrared reflection) analysis: As a supplementary method, FTIR technique was adopted to identify the primary crystalline phases in the glass-ceramic and extent of crystallisation. The specimens from different stages of heat treatment were cut into 10×10×3 (mm) plates, polished with 3 μm CeO_2 abrasive and ultrasonic cleaned in acetone for 5 min. The specimens were tested under FTIR spectrometer (Nicolet, Magna-IR^{TM} Spectrometer 550, America).

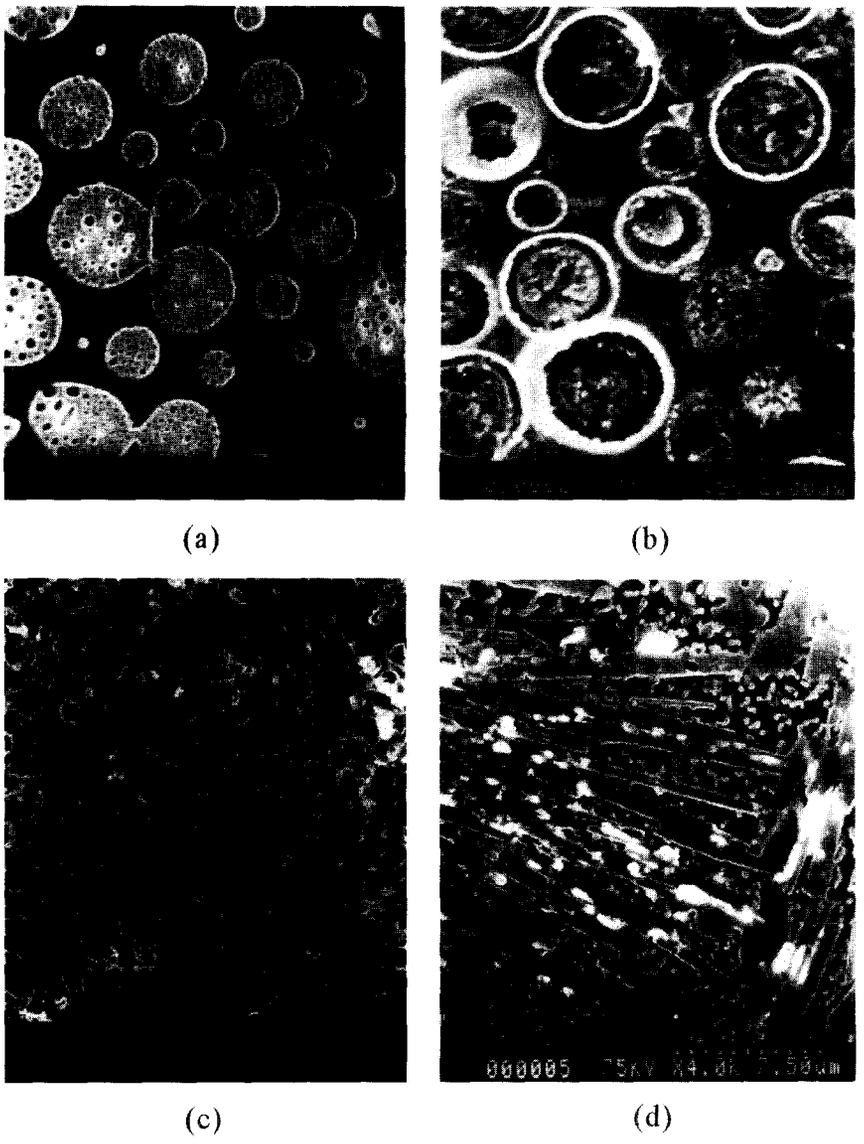

Fig. 3. SEM photographs of the specimens of the glass G1 with different stages of heat treatment. (a) G1-0; (b) G1-1; (c) G1-2 and (d) G1-3.

3 RESULTS AND DISCUSSION

3.1 Glass-in-glass phase separation

Figures 3(a), 4(a) and 5(a) show that multiple glass-in-glass phase separation occurred in all three original glasses—G1-0, G2-0, and G3-0, but the morphologies of phase seperation were quite different. In G1-0, many spherical phases are embedded in a continuous glassy matrix phase, and a large number of fine droplets are secondarily separated from the spherical phases (the primary separated phases). In G2-0 and G3-0 which contained a higher content of $CaO+P_2O_5$ than G1-0, there coexist four phases: (1) the irregular interconnected phases(the primary separated phases); (2) the matrix phases, (3) the spherical phases embedded in the matrix phases and (4) fine droplets separated from the primary separated phases.

Figure 6 shows the SEM of the phase separation morphology of G1-0 (corresponding to Fig. 3(a)) and the EDAX spectra of the different regions of phase separation. The EDAX test indicated that the spherical primary separated phases had a relatively high concentration of P, Ca and Ti elements, whereas the matrix phase contained comparatively high concentrations of Si, Al and K elements.

The phase separation in this system can be explained as follows:

(1) From the point of view of crystal chemistry, the ionic field strength F can be described as:[7]

$$F = Z/r_2 \tag{1}$$

where F is the ionic field strength, Z the ionic valence and r the ionic radius.

P^{5+} ion has a higher ionic field strength than Si^{4+} ion (43.2 compared to 23.8). Therefore, P^{5+}

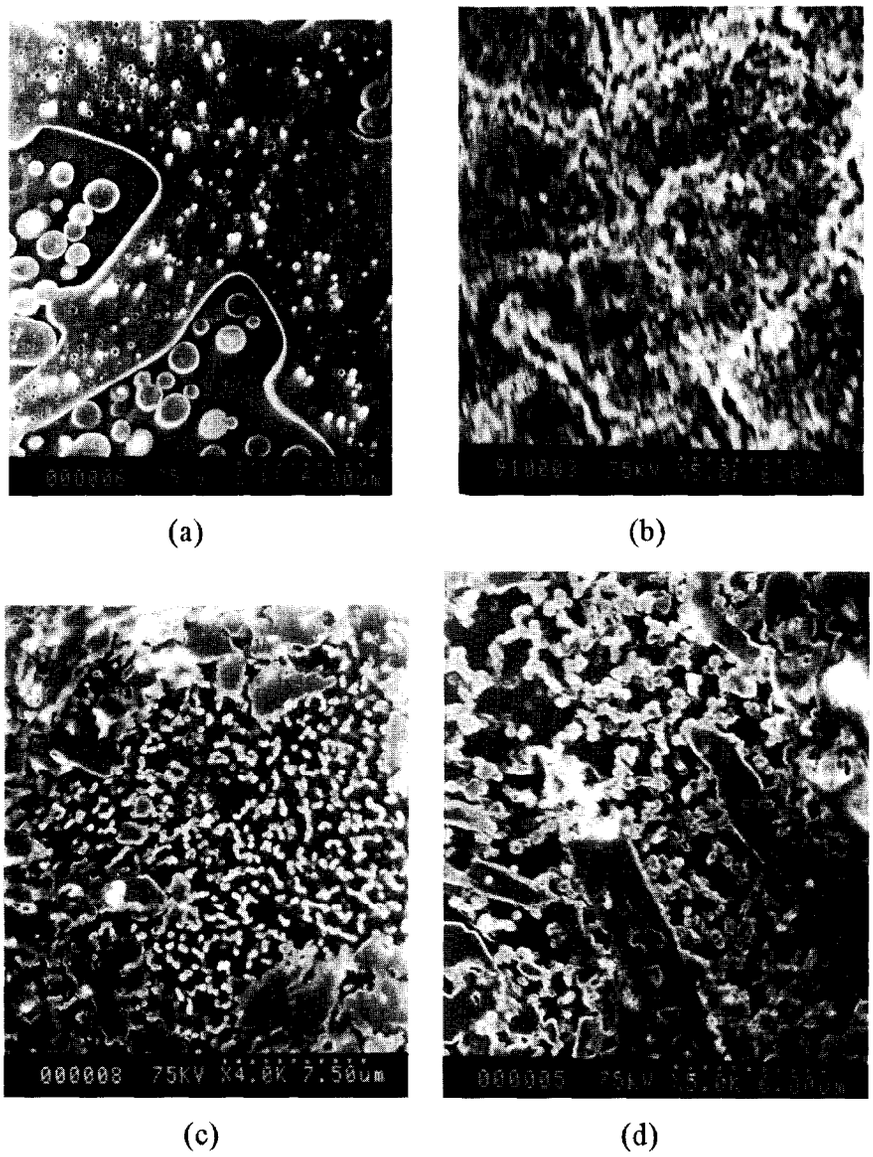

Fig. 4. SEM photographs of the specimens of the glass G2 with different stages of heat treatment. (a) G2-0; (b) G2-1; (c) G2-2 and (d) G2-3.

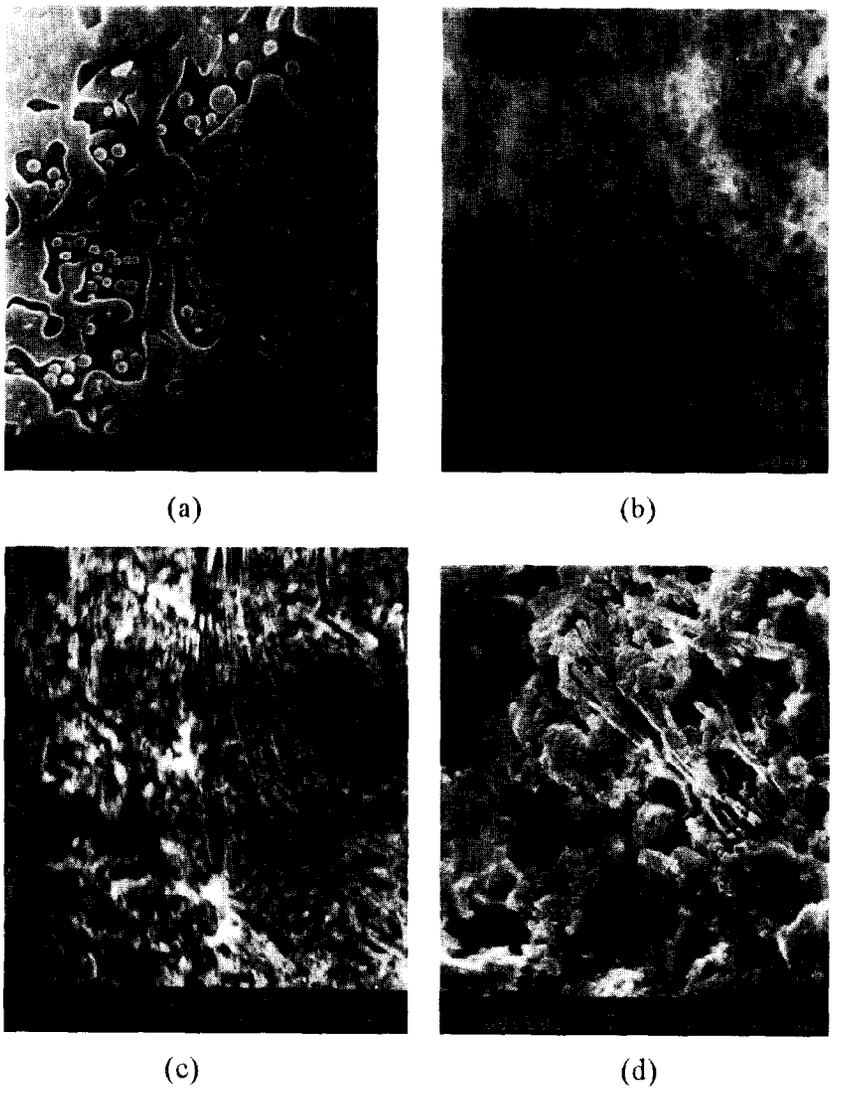

Fig. 5. SEM photographs of the specimens of the glass G3 with different stages of heat treatment. (a) G3-0; (b) G3-1; (c) G3-2 and (d) G3-3.

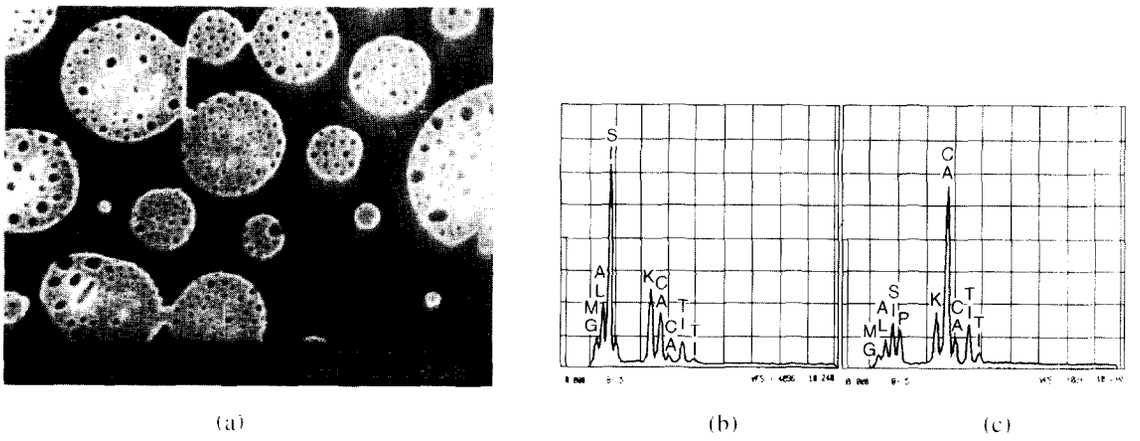

Fig. 6. The SEM photograph of (a) G1-0 and its EDAX spectra corresponding to different regions of phase separation: (b) the matrix phase; (c) the spherical phases.

ions can coordinate more O^{2-} ions from the silicate network which is rather open due to various interstitial or modifying cations and contains a large amount of 'free oxygens.' Since P^{5+} is a pentavalent network forming cation, electroneutrality is ensured only if one of the four oxygen ions around P^{5+} ion is doubly bonded to the central P^{5+} cation as shown schematically in Fig. 7. The double bond in the PO_4 tetrahedra is shorter in length than other three single bonds (1.424Å compared to

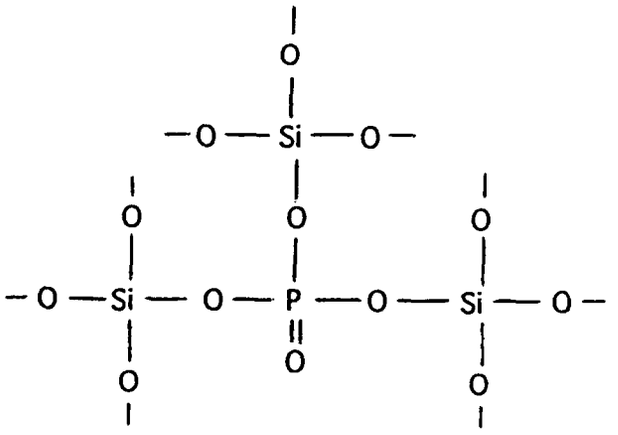

Fig. 7. Possible arrangement of silicate networks containing P^{5+} network forming cations.

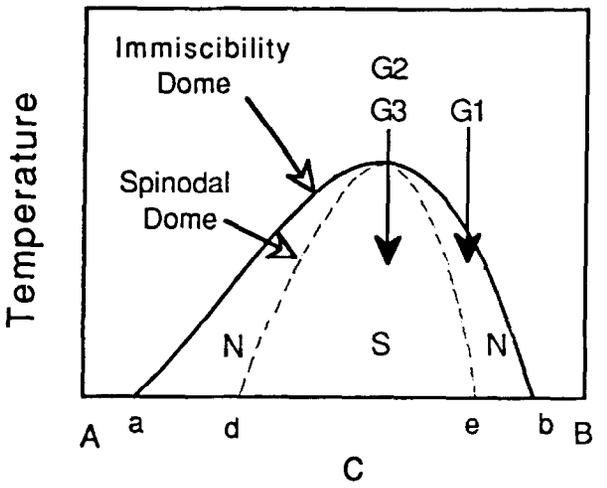

Fig. 8. Schematic illustration of the immiscibility gap. A: P_2O_5+CaO; B: $SiO_2+Al_2O_3+MgO+K_2O$; S: spinodal region; N: binodal region (or nucleation and growth region).

1.595Å), which results in asymmetry of the PO_4 tetrahedron and disturbs the bonding in the silicate network. Under these circumstance, phase separation is likely to occur, and the phosphate-rich and silicate-rich phases are separated from the parent glass. More Ca^{2+} and Ti^{4+} cations are included in the phosphate-rich phase because P^{5+} ion has a higher ionic field strength and hence a greater tendency to shielding[5] (see Fig. 6(c)).

(2) Thermodynamically, the phase separations occurring in the G1-0, G2-0 and G3-0 glasses correspond to different mechanisms of immiscibility. The change in the free energy (ΔG) of the system with localised compositional fluctuations over a perfectly homogeneous system can be approximately given by the following equation (neglecting higher-order terms):[8]

$$\Delta G = G(c) - G(\bar{c}) = (l/2)(\mathrm{d}^2G/\mathrm{d}^2)\int_v h^2\,\mathrm{d}v \qquad (2)$$

where h is an infinitesimal fluctuation in composition about the mean composition; $\bar{c}$ is the composition after fluctuation. Equation (2) is applicable for a binary A–B system.

To simplify the system, we suggest that in the studied system, A represents P_2O_5+CaO and B represents $SiO_2+Al_2O_3+MgO+K_2O$. The phase separation behaviour can thus be described schematically as in Fig. 8.

For G1-0, the composition lies in the binodal region, where we have $\mathrm{d}^2G/\mathrm{d}c^2>0$, thus $\Delta G>0$ from eqn (2). In this case, for the fluctuational formation of an inhomogeneity region capable of further stable development it is necessary to overcome a free energy barrier. The primary phase separation in G1-0 was reached through the mechanism of so called "binodal decomposition" or "nucleation and growth",[8,9] which formed spherical phosphate-rich phases with a low connectivity and the matrix phase containing a relatively high content of the silicates (Fig. 3(a)). On the other hand, compositions G2-0 and G3-0 fell in the spinodal region, where $\mathrm{d}^2G/\mathrm{d}c^2<0$, hence $\Delta G<0$. The concentration fluctuations, no matter how weak they are, are capable of developing by lowering the free energy leading to primary phase separations through the mechanism of "spinodal decomposition." The primary separated phases rich in the phosphates assumed wormlike morphologies, possessed high connectivities and a volumetric ratio to the matrix phases which was rich in silicates (Figs 4(a) and 5(a)).

There are also secondary phase separations in the studied glasses (Figs 3(a), 4(a) and 5(a)). Mazurin and Porai-Koshits[9] indicated that secondary phase separation in each of the primary phases proceeds at different rates which can be affected by two factors: (1) different degrees of supersaturation of the phases, due to asymmetry of the ΔG-X curve; (2) differences between the viscosities and hence between the interdiffusion coefficients, of the primary phases. As a result, secondary phase separation is often observed only in one phase, e.g. in G1-0, no obvious evidence of secondary phase separation was found in the silicate-rich matrix phase which had a higher viscosity than the phosphate-rich spherical phases where secondary phase separation occurred.

The stepwise immiscibility in the glasses G1-0, G2-0 and G3-0 is schematically illustrated in Fig. 9. It can be seen from Fig. 9 that the phosphate-rich side rises gently, but the silicate-rich side rises relatively steeply due to the asymmetry of the immiscibility dome of the studied system. This means that the solubility of silicates in the phosphate-rich phase rapidly decreased with falling temperature.

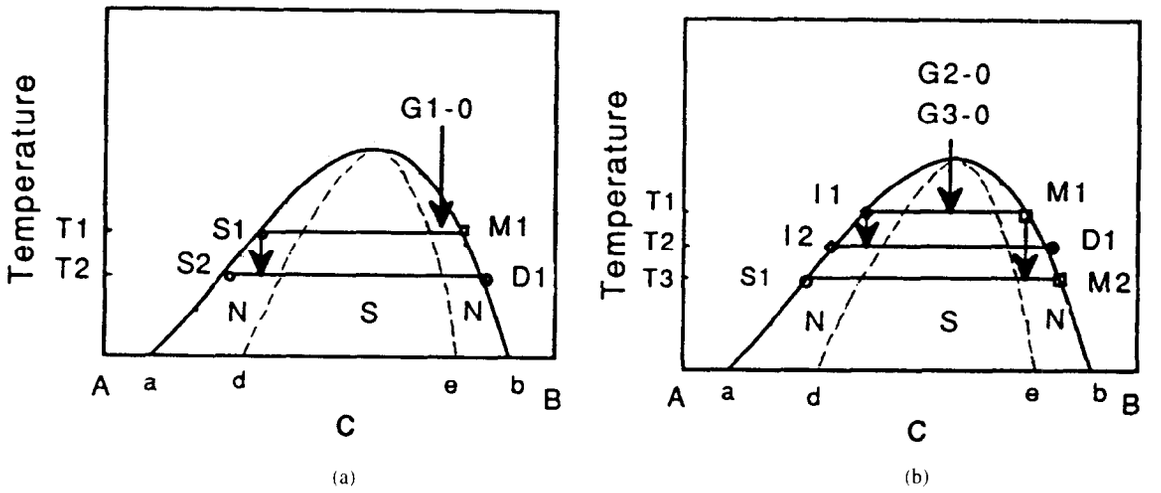

Fig. 9. The schematic illustration of the stepwise immiscibility of the studied system. (a) G1-0 (S: the spherical phase; M: the matrix phase; D: the fine droplet); (b) G2-0 and G3-0 (I: the irregular interconnected phase; M: the matrix phase; S: the spherical phase; D: the fine droplet).

Figure 9(a) shows that the ultimate three phases which resulted from secondary phase separation in G1-0 are: (1) the matrix phase Ml, rich in silicates; (2) the spherical phase S2 which consists of primary separated phases derived from Sl and are rich in phosphate. According to the lever rule,[9] it can be easily understood that S2 possesses a lower volumetric ratio to Ml than that of the phosphate-rich phase in G2-0; (3) the fine droplets Dl which were separated secondarily from the spherical phases Sl and contained a comparatively high concentration of silicate. Figure 9(b) illustrates that there coexist four ultimate phases in G2-0 and G3-0 due to secondary phase separation, which are: (1) the matrix phases M2 rich in silicates; (2) the irregular interconnected phases *I2* derived from *Il* which are the original separated-phases rich in phosphate. According to the lever rule, the volumetric ratio of the phosphate-rich phases (I2) to the silicate-rich phases (M2) in G2-0 and G3-0 are larger than in G1-0 (i.e. S2 to M1); (3) the spherical phases Sl secondarily separated from the matrix phase which contain a higher concentration of phosphate than the matrix phases; (4) the fine droplets Dl secondarily separated from the irregular phases *I2* but with a higher concentration of silicates than that of *I2*.

3.2 The relationship between phase separation, nucleation and clystallization

Phase separation and crystallisation are independent phase transformation processes. However, almost every controlled crystallisation of glass has as its basis and prerequisite a controlled phase separation.[5] Our study indicates that the phase separations in the studied system can facilitate crystal nucleation in the different phases.

The nucleation rate (I) in glass may be written as[7]

$$I = A\exp[-(\Delta F^* + Q)/KT] \qquad (3)$$

where I is nucleation rate, A is a constant, Q is activation energy for diffusion of molecules across the phase boundary, ΔF^* is maximum free energy of activation for formation of a stable nucleus.

In the glasses Gl-0, G2-0 and G3-0, the phase separations occurring can result in a selective enrichment of elements in different phases, which make the compositions and structures of certain phases more similar to the main crystalline phases than that of the initial glasses. For instance, the primary separated phase rich in phosphate in the studied glasses was closer in composition to the stoichiometry of apatite than the ideally homogeneous glasses, and the composition of the matrix phases rich in silicates were relatively similar to that of phlogopite. In this case, the thermodynamic and kinetic potential barriers for crystal nucleation (ΔF^* and Q in eqn (3)) can be decreased and hence the nucleation rate(I) increased. This also means that the tendency of the glass towards crystallisation can be enhanced.

In addition, development of a large amount of interfacial area can afford abundant nuclei with a range of surface energies, which is necessary for formation of crystal nucleation.

From Fig. 3(b), it can be seen that the nuclei of fluorapatite are initially formed in the spherical phosphate-rich phases in Gl-0, and the nuclei of fluorophlogopite are formed first in the silicate-rich matrix phase.

3.3 Crystallization of the glasses

Figures 3(d), 4(d) and 5(d) show that there coexist two main crystalline phases in the resultant glass ceramics—Gl-3, G2-3 and G3-3. One crystalline phase possesses lamellar(for G1-3 and G2-3) or flake-like(for G3-3) morphologies, and their sizes along the major axis direction range from 10 to 15 μm. Another main crystalline phase assumes a fine granular morphology with sizes around 0.3–0.5 μm. A great number of fine granular microcrystals distribute around the lamellar (or flake-like) crystals with random orientation. The analyses of XRD (Fig. 10), FTIR (Fig. 11) and SEM/EDAX (Fig. 12) indicated that the lamellar (or flake-like) microcrystals were fluorophlogopite ($KMg_3(AlSi_3O_{10})F_2$, monoclinic crystal system), and the fine granular crystals were fluorapatite ($Ca_5(PO_4)_3F$, hexagonal crystal system). Their microstructures are illustrated schematically in Fig. 13.

It is indicated in Figs 3–5, 10 and 11 that the microcrystals of fluorapatite and fluorophlogopite are crystallised at different temperatures. The former are nucleated in the primary separated phases rich in phosphates at Stage 1 (650°C 1 h^{-1}) and crystallised at Stage 2 (770–800°C 3 h^{-1}). The latter were initially formed in the matrix phases rich in silicates at Stage 2 by epitaxial growth on norbergite microcrystallites (Figs 3(c) and 10). At this stage, the morphologies of the mica crystallites were not very typical. The more perfect mica crystals were formed at Stage 3 (850–930°C 3 h^{-1}). In fact, the mica crystals can be precipitated at any temperature between 850°C and 1050°C. The glass Gl has a lower crystallisation temperature for the mica and a higher crystallisation temperature for the apatite than the glass G2 and G3, due to its lower content of $CaO + P_2O_5$. This is also indicated by the DTA curves of the glasses shown in Fig. 1. The first and the second exothermic peaks in the DTA curves, respectively, represent the crystallisation temperatures of fluorapatite and fluorophlogopite. The growth rate and size of the mica crystals will be increased with a higher soaking temperature and prolongation of the soaking time for crystallisation. The glass-ceramics will be softened and deformed if the soaking temperature is over 1050°C.

From Fig. 13(a) it can be seen that the alkali ions are sandwiched between the three-layer packets which results in very weak connections between the layers. The (001) plane of the mica crystals will be preferred as a direction of cleavage when the glass-ceramics are machined. Due to a great number of interlocking mica crystals in the glass-ceramics, the microfractures caused by mechanical processing easily propagate from crystal to crystal, resulting in removal of material without breaking the part.[5]

With the increase of the $CaO + P_2O_5$ content, the number of the mica crystals are decreased without obvious size change (Fig. 4(d)). Therefore, the machinability of G2-3 glass-ceramic is not as good as that of G1-3.

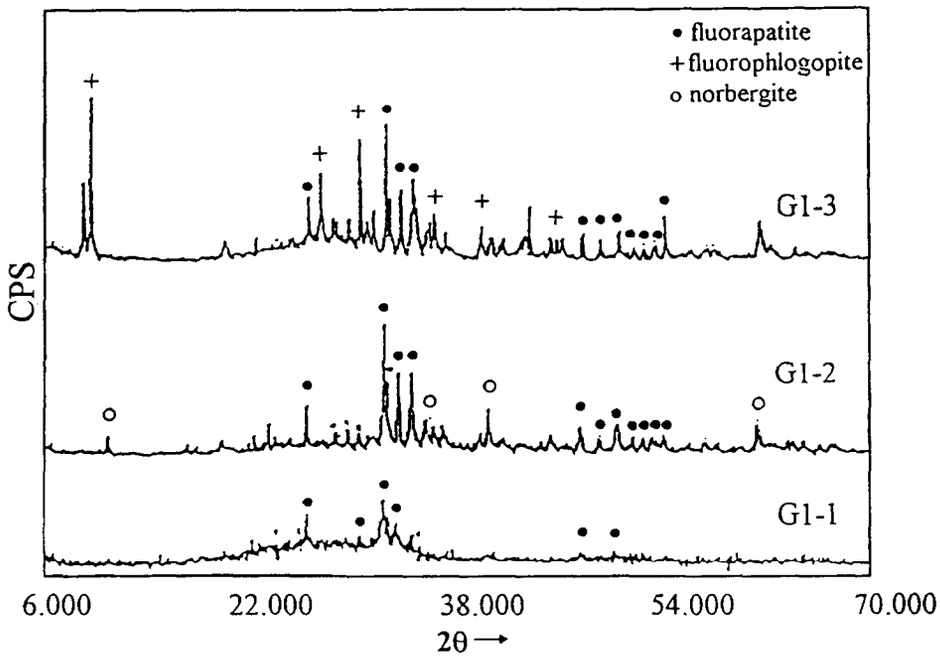

Fig. 10. XRD patterns of the specimens of the glass Gl corresponding to different stages of heat treatment (see Fig. 2 and Table 3). It is shown that the two main crystalline phases are crystallised at different temperatures. (The corresponding micromorphologies of these specimens are shown in Fig. 3).

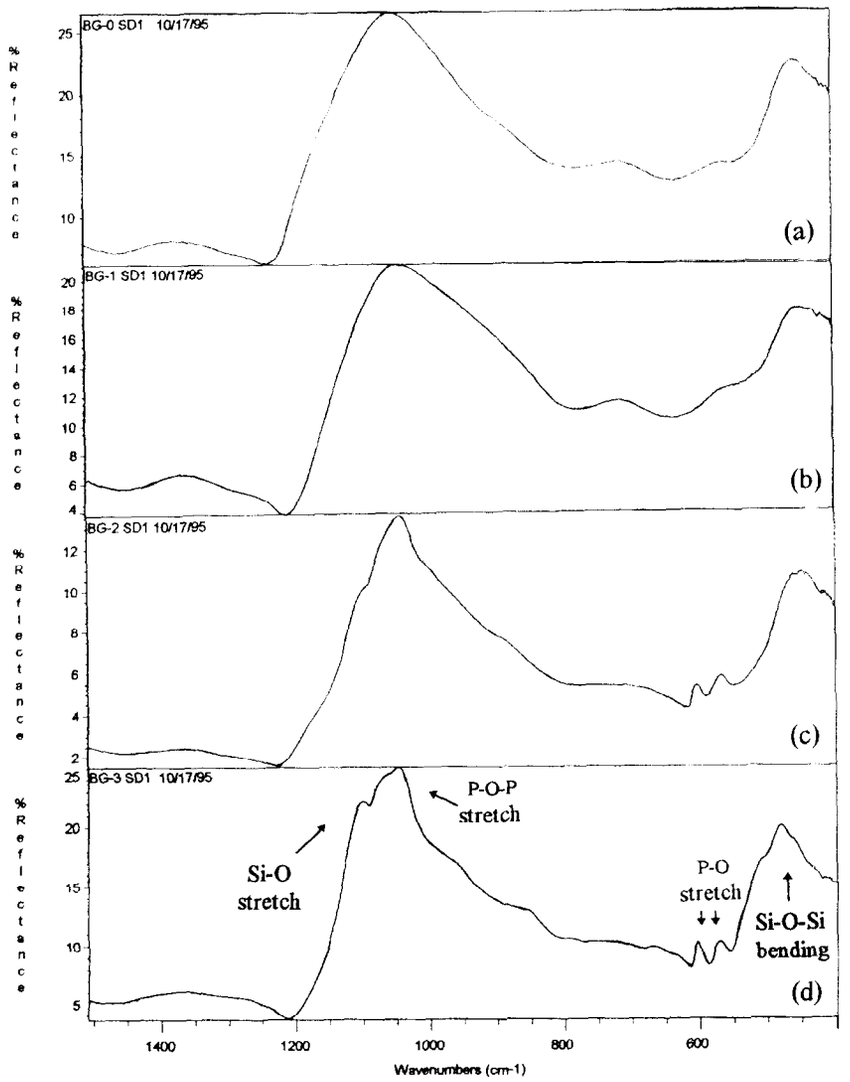

Fig. 11. FTIR spectra of the specimens of the glass G1 corresponding to different stages of heat treatment. (a) G1-0; (b) G1-1; (c) G1-2 and (d) G1-3. The spectra illustrate that fluorapatite crystals were formed in Stage 2 ((c) 800°C 3 h $^{-1}$), and fluorophlogopite crystals were crystallised in Stage 3 ((d) 850°C 3 h^{-1}).

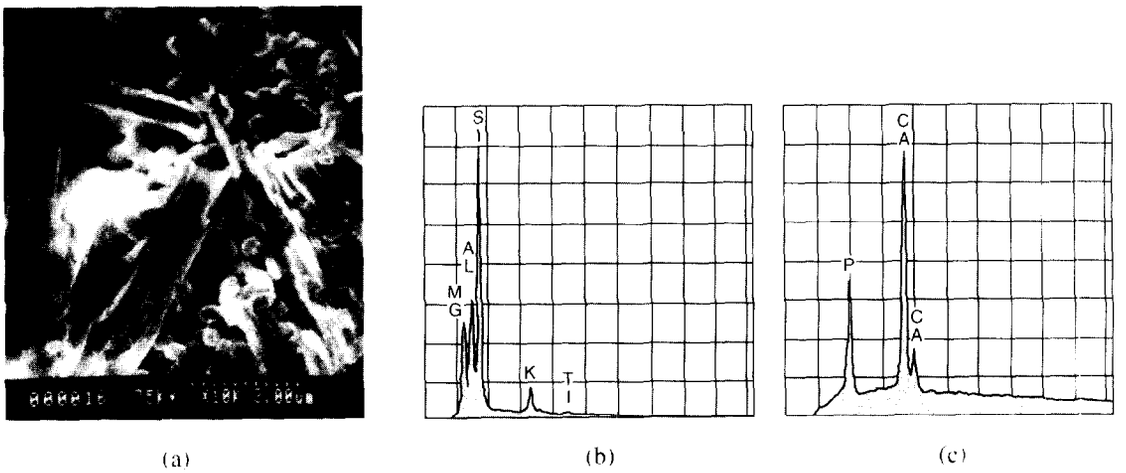

Fig. 12. SEM photograph of G1-3(a) and EDAX spectra of the two crystalline phases: (b) fluorophlogopite and (c) fluorapatite.

Bioactivity and biocompatibility of the studied glass-ceramic was investigated by means of *in vitro* and *in vivo* in our previous work.[6,10] A hydroxylapatite crystalline layer incorporated with CO_3^{2-} could form on the material surfaces in simulated body fluid (SBF) at 37°C. The experiment of implantation into animals showed that the glass-ceramic directly bonded to surrounding bone due

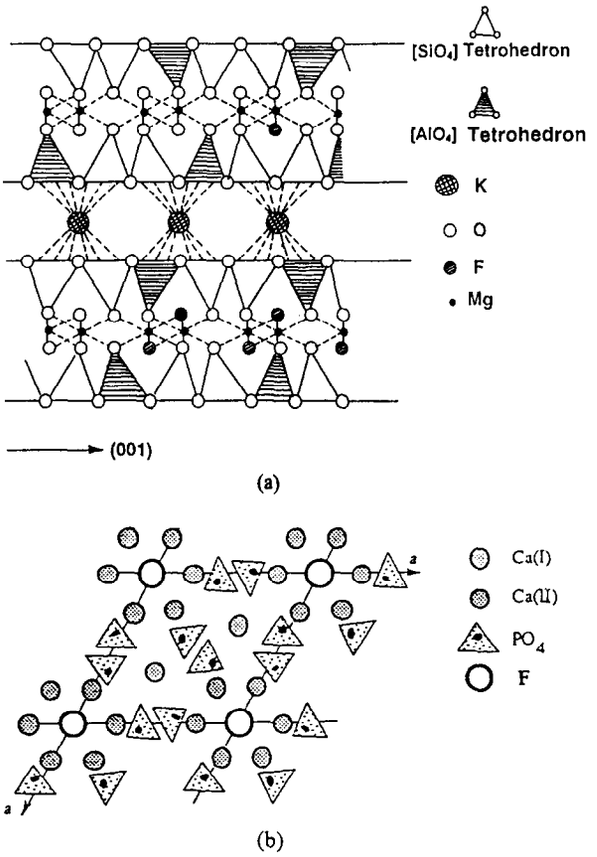

Fig. 13. Diagrams of the microstructures of fluorophlogopite (a)[5] and fluorapatite (b).[10]

to formation of a firm chemical bond between the bone and the glass-ceramic implant.

4 CONCLUSION

The phase separations occurring in the glasses of the system K_2O–MgO–CaO–Al_2O_3–B_2O_3–SiO_2–P_2O_5–F correspond to different mechanisms of immiscibility. For the glass with a lower content of P_2O_5+CaO, the primary phase separation is reached through binodal decomposition or nucleation and growth. For the glass with a higher content of P_2O_5+CaO, the primary phase separation is led by spinodal decomposition. The two mechanisms result in different micromorphologies of the glasses.

The secondary phase separation in glasses are favourable for the nucleation of fluorophlogotite and fluorapatite microcrystals due to: (1) the similarity of compositions and structures between the glassy phases and the corresponding crystalline phases; (2) the large amount of phase interfaces yielded by secondary phase separations which can decrease the thermodynamic and kinetic potential barriers for nucleation of crystals.

The microcrystals of fluorophlogopite with lamellar structure are primarily precipitated in the matrix phases rich in silicates at a higher temperature (850–1050°C) than fluorapatite (770–800°C). The fluorapatite microcrystals are initially nucleated in the phosphate-rich phases.

The glass-ceramics containing the fluorophlogopite and fluorapatite microcrystals possess biocompatibility, bioactivity and machinability. These biomaterials can be easily processed into prosthetic devices with different shapes for clinical applications.

ACKNOWLEDGEMENTS

The authors would like to thank G. P. LaTorre for experimental assistance, helpful discussions and reading the manuscript. This work was supported in part by U.S. Biomaterials Corporation.

REFERENCES

1. HENCH, L. L., *J. Am. Ceram. Soc.*, **74**(7) (1991) 1487–1510.
2. HENCH, L. L. & WILSON, J. (ed.), *An Introduction to Bioceramics*. World Scientific Publishing Co. Pte. Ltd, Singapore, 1993.
3. RAWLINGS, R. D., *Clinical Materials*, **14** (1993) 155–179.
4. HENCH, L. L., *Bioceramics*, Vol. 7. Proceedings of the 7th International Symposium on Ceramics in Medicine, Turku, 1994, pp. 8–12.
5. HÖLAND, W. & VOGEL, W., in *Introduction to Bioceramics*. World Scientific, Singapore, 1993, pp. 125–137.
6. CHEN, X. F., ZHANG, X. K., TENG, L. D. & ZHANG, M. M., *J. Chin. Ceram. Soc.*, **21**(3) (1993) 247–255.
7. McMILLAN, P. W., *Glass-Ceramics*. Academic Press Inc., London, 1979.
8. VARSHNEYA, A. K., *Fundamentals of Inorganic Glasses*. Academic Press, Inc., San Diego, 1994.
9. MAZURIN, O. V. & PORAI-KOSHITS, E. A., *Phase Separation in Glass*. North-Holland Physics Publishing, Amsterdam, 1984.
10. ZHANG, X. K., CHEN, X. F. & HUANG, P., *X-Ray Optics and Microanalysis 1992*. IOP Publishing Ltd, London, 1993, pp. 205–208.